

Exploring Low-Loss Surface Acoustic Wave Devices on Heterogeneous Substrates

Jinbo Wu¹, Graduate Student Member, IEEE, Shibin Zhang¹, Member, IEEE, Liping Zhang, Graduate Student Member, IEEE, Hongyan Zhou, Graduate Student Member, IEEE, Pengcheng Zheng, Graduate Student Member, IEEE, Hulin Yao, Zhongxu Li, Kai Huang, Tao Wu¹, Senior Member, IEEE, and Xin Ou¹, Member, IEEE

Abstract—This article presents shear horizontal surface acoustic wave (SH-SAW) devices with excellent temperature stability and low loss on ultrathin Y42-cut lithium tantalate film on sapphire substrate (LiTaO₃-on-sapphire, LTOS). The demonstrated resonators exhibit scalable resonances from 1.76 to 3.17 GHz, effective electromechanical coupling coefficients between 5.1% and 7.6%, and quality factors (Bode- Q) between 419 and 3019. The filter with a center frequency of 3.26 GHz features a suppressed spurious passband, a 3-dB fractional bandwidth (FBW) of 3%, and a minimum insertion loss (IL) of 2.39 dB. In addition, coplanar waveguides (CPWs) and SH-SAW resonators built on LTOS and LiTaO₃-on-insulator (LTOI) substrates were compared over a temperature range of 25 °C–150 °C. Due to the extremely high resistivity of the sapphire and the excellent thermal stability of the LiTaO₃/sapphire interface, the IL of the CPW and the impedance ratio (in addition to Bode- Q) of

the SH-SAW on the LTOS are maintained well even at 150 °C, while those on the LTOI seriously deteriorate. Of these, the impedance attenuation of LTOS-SAW at the antiresonant frequency is only 3.7 dB at 150 °C, whereas that of LTOI-SAW reaches 9.6 dB, demonstrating excellent temperature stability of the LTOS substrate's radio frequency (RF) performance. Overall, the SAW devices on LTOS substrates show great potential for temperature-sensitive and low-loss applications in RF wireless communications.

Index Terms—LiTaO₃-on-sapphire (LTOS), piezoelectric filter, radio frequency (RF) loss, shear horizontal (SH) mode, surface acoustic wave (SAW) resonator.

I. INTRODUCTION

ACOUSTIC devices are widely used in radio frequency (RF) wireless communications for frequency selection and interference suppression. Surface acoustic wave (SAW) resonators dominate the RF filter market [1]–[7] due to their low cost, simple structure, and lithography-defined operating frequency [8], [9]. For applications within the increasingly crowded frequency bands of mobile communication systems, advanced SAW filters with steeper skirts and lower insertion loss (IL) are urgently required. The quality factor (Q) is a key factor involved in achieving the desired performance in these devices. When SAW devices are correctly designed, the Q value will be improved due to the reduction of the intrinsic loss of the (heterogeneous) piezoelectric substrate and enhancement of the acoustic energy confinement.

In recent years, acoustic devices using lithium tantalate (LiTaO₃) and lithium niobate (LiNbO₃) thin films on heterogeneous substrates have achieved breakthrough performance [6], [7], [10]. The incredible high-performance SAW (I.H.P.-SAW), generally built on LiTaO₃/SiO₂/Si (LiTaO₃-on-insulator, LTOI) substrate as shown in Fig. 1(a), achieves excellent Q values [2], [11]–[13]. The SiO₂/Si structure can reflect and confine acoustic energy inside the LiTaO₃ thin film. However, the fabrication process of the LTOI substrate must be precisely controlled; if not, fixed positive charges inside the SiO₂ dielectric layer will attract free carriers of the silicon supporting substrate, thus resulting in the parasitic surface conduction (PSC) effect at the SiO₂/Si interface [14]–[19]. In such a case, the effective resistivity of the high-resistance silicon (HR-Si) substrate surface will be reduced by more than one order of magnitude, resulting in additional RF loss

Manuscript received 31 March 2022; accepted 30 May 2022. Date of publication 2 June 2022; date of current version 29 July 2022. This work was supported in part by the China Postdoctoral Science Foundation under Grant 2021M703339; in part by the Shanghai Post-Doctoral Excellence Program under Grant 2020487; in part by the National Key Research and Development Program of China under Grant 2020YFB2008802 and Grant 2019YFB1803903; in part by the National Natural Science Foundation of China under Grant 61874128, Grant 61851406, Grant 11705262, and Grant 61874073; in part by the Frontier Science Key Program of CAS under Grant QYZDY-SSW-JSC032 and Grant ZDBS-LY-JSC009; in part by the Chinese–Austrian Cooperative Research and Development Project under Grant GJHZ201950; in part by the Program of Shanghai Academic Research Leader under Grant 19XD1404600; and in part by the K. C. Wong Education Foundation under Grant GJTD-2019-11. (Jinbo Wu and Shibin Zhang contributed equally to this work.) (Corresponding authors: Shibin Zhang; Xin Ou.)

Jinbo Wu is with the State Key Laboratory of Functional Materials for Informatics, Shanghai Institute of Microsystem and Information Technology, Chinese Academy of Sciences, Shanghai 200050, China, also with the Center of Materials Science and Optoelectronics Engineering, University of Chinese Academy of Sciences, Beijing 100049, China, and also with the School of Information Science and Technology (SIST), ShanghaiTech University, Shanghai 201210, China.

Shibin Zhang and Kai Huang are with the State Key Laboratory of Functional Materials for Informatics, Shanghai Institute of Microsystem and Information Technology, Chinese Academy of Sciences, Shanghai 200050, China (e-mail: sbzhang@mail.sim.ac.cn).

Liping Zhang, Hongyan Zhou, Pengcheng Zheng, Hulin Yao, Zhongxu Li, and Xin Ou are with the State Key Laboratory of Functional Materials for Informatics, Shanghai Institute of Microsystem and Information Technology, Chinese Academy of Sciences, Shanghai 200050, China, and also with the Center of Materials Science and Optoelectronics Engineering, University of Chinese Academy of Sciences, Beijing 100049, China (e-mail: ouxin@mail.sim.ac.cn).

Tao Wu is with the School of Information Science and Technology (SIST), ShanghaiTech University, Shanghai 201210, China.

Digital Object Identifier 10.1109/TUFFC.2022.3179699

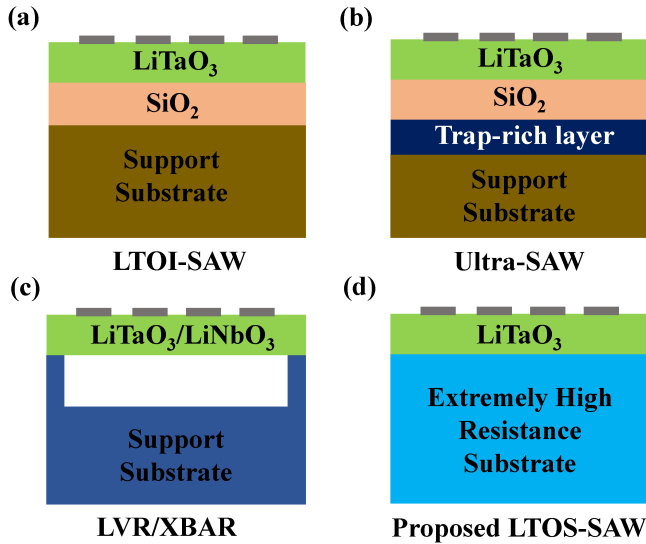


Fig. 1. Schematics of (a) LTOI-SAW, (b) Ultra-SAW, (c) LVR/XBAR, and (d) proposed LTOS-SAW.

and Q value degradation. SAW devices based on the smart-cut piezo on insulator structure (also known as Ultra-SAW) represent another type of high- Q device; these devices feature a trap-rich layer (e.g., poly-Si) inserted between the SiO_2 layer and the Si substrate to mitigate the PSC effect as shown in Fig. 1(b) and have exhibited maximum Bode- Q [20] (Q_{\max}) values of around 6000 [3], [21]. However, the substrate structure and fabrication process are more complicated and costly in this configuration. Taking advantage of the large acoustic impedance mismatch between the air and the piezoelectric thin film, the laterally vibrating resonator (LVR) [22]–[27] and the laterally excited bulk acoustic wave resonator (XBAR) [28], [29] using released LiNbO_3 thin films can effectively confine the acoustic energy in LiNbO_3 thin films, resulting in a relatively high Q . As shown in Fig. 1(c), the LVR (XBAR) configuration has a simple structure and can eliminate the PSC effect. However, suspended devices exhibit intrinsically poor power capacity, large temperature coefficient of frequency, and fragile structures, which limit their practical applications. Since solidly mounted acoustic devices require complex, multilayered substrates to obtain high Q values, suspended devices with simple structures can achieve high Q values but limited performance in other regards. On this basis, a key question remains—is there a heterogeneous substrate with a simple structure that can effectively confine acoustic energy and eliminate the PSC effect for building low-loss devices?

In this study, a single-crystalline Y42-cut LiTaO_3 thin film was transferred onto a sapphire substrate [LTOS, as shown in Fig. 1(d)] by the ion-cutting process [30]. Coplanar waveguides (CPWs) built on LTOS show smaller IL (RF loss) than those built on LTOI substrates. A series of SH-SAW resonators with various λ (where λ is the period of the interdigital transducer [31]) were designed and fabricated on LTOS substrates, showing scalable resonances from 1.76 to 3.17 GHz and Q_{\max} of around 3000. The Rayleigh mode

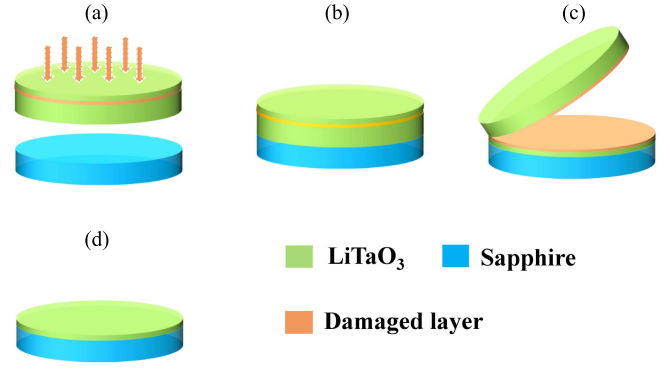


Fig. 2. Process flow of preparing the LTOS substrate by the ion-cutting process: (a) ion implantation, (b) wafer bonding, (c) annealing and splitting, and (d) chemical-mechanical polishing (CMP).

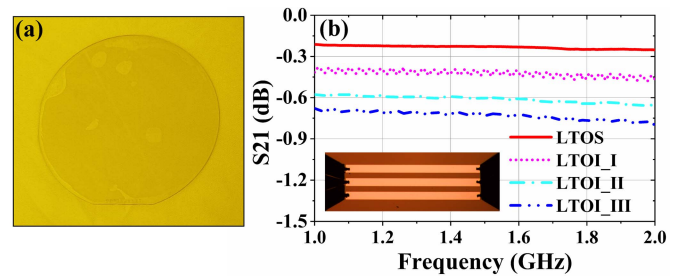


Fig. 3. (a) Photograph of the fabricated LTOS wafer. (b) OM image of a fabricated CPW (see inset) and the IL (S_{21}) per 2 mm of CPW built on the LTOS substrate, as well as three LTOI substrates with different postannealing conditions.

spurious responses of the demonstrated resonators and filters were effectively suppressed. The fabricated ladder-type filter shows a spurious passband-free response, high operating frequency, and low IL. In addition, the IL of the CPW built on the LTOS substrate remained small at 150 °C, with only a slight Q value decrease for LTOS-SAW recorded at this high temperature, thus indicating the stable RF performance of the LTOS substrate.

This article is an extension of [32], which reports the first trial of the resonator and low-order filter based on LTOS. In this article, CPWs were introduced to characterize the RF loss, groups of acoustic devices were designed and measured, high-temperature testing was performed to demonstrate the thermal stability of the sapphire substrates' RF performance, and the key parameters of the groups of devices were extracted and analyzed to further explore the properties of the LTOS substrate.

II. STUDY OF LTOS SUBSTRATE

The ultrathin Y42-cut LiTaO_3 film was transferred to the sapphire substrate using the ion-cutting process, with the process flow shown in Fig. 2. After chemical-mechanical polishing (CMP), the thickness of the Y42-cut LiTaO_3 thin film was reduced to 460 nm, with an image of the 4-in LTOS wafer shown in Fig. 3(a).

To characterize the RF loss of the LTOS substrate, the CPWs were built on the LTOS and three other LTOI substrates

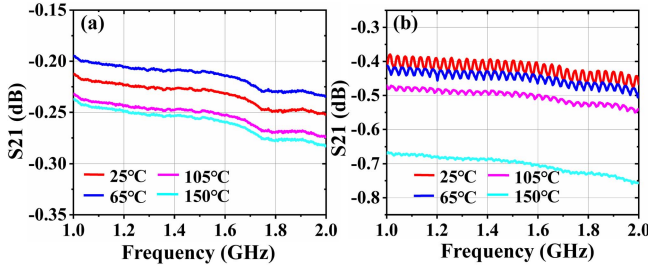


Fig. 4. Temperature characteristics of CPWs built on (a) LTOS and (b) LTOI_I substrates.

with varying postannealing conditions. The structure of the LTOI substrates is shown in Fig. 1(a), and the thicknesses of the Y42-cut LiTaO₃ film and SiO₂ layer are 600 and 500 nm, respectively. An optical microscope (OM) image and the measured IL (S21) per 2 mm of CPWs are shown in Fig. 3(b). As a result of the extremely high resistivity of the sapphire supporting substrate [33], the LTOS substrate shows a much smaller IL (i.e., RF loss) than those of the LTOI substrates. In particular, the difference (S21) between the LTOS and LTOI_I substrates generated under the same fabrication process is mainly caused by the PSC effect.

Subsequently, the CPWs built on the LTOS and LTOI_I substrates were tested at higher temperatures, with the measured results shown in Fig. 4(b). Both substrates showed increased IL with rising temperatures. When the test temperature reached 150 °C, the IL of the LTOS substrate remained small, whereas the IL of the LTOI substrate increased substantially. This shows that the LTOS substrate still exhibits low RF loss at higher temperatures. Furthermore, compared to LiTaO₃, sapphire has a smaller thermal expansion coefficient [33], larger thermal conductivity, and higher acoustic velocity [6], the combination of which helps to further improve the device performance.

III. DESIGN OF LTOS-SAW DEVICES

To analyze the dispersion characteristics of the SH-SAW and Rayleigh mode (spurious response), resonators on LTOS with different λ -values ($1.2 \leq \lambda \leq 2.6 \mu\text{m}$) were simulated using the 3-D finite element analysis (FEA), with the corresponding admittance curves and extracted k_{eff}^2 values shown in Fig. 5(a) and (b), respectively. The displacement mode shapes of the SH-SAW and Rayleigh mode are shown in Fig. 5(c). The simulation model comprises 60 pairs of interdigital transducer (IDT) electrodes and 25 pairs of reflectors on both sides, with perfect matching layers set on both sides and the bottom of the model. The thicknesses of the aluminum electrode (h_{Al}) and LiTaO₃ (h_{LT}) are set to 135 and 460 nm, respectively. k_{eff}^2 is given by $k_{\text{eff}}^2 = \pi^2/8 \times (f_p^2 - f_s^2)/f_s^2$, where f_s and f_p are the resonance and antiresonance frequencies, respectively [34]. k_{eff}^2 of SH-SAW achieves its maximum value of 10.4% when $\lambda = 1.6 \mu\text{m}$, the resonance frequency of the Rayleigh mode is always lower than that of the SH-SAW, and the k_{eff}^2 value of the Rayleigh mode decreases to zero as λ decreases. Accordingly, a resonator on the LTOS substrate with a moderate k_{eff}^2 and without Rayleigh mode spurious response can be expected

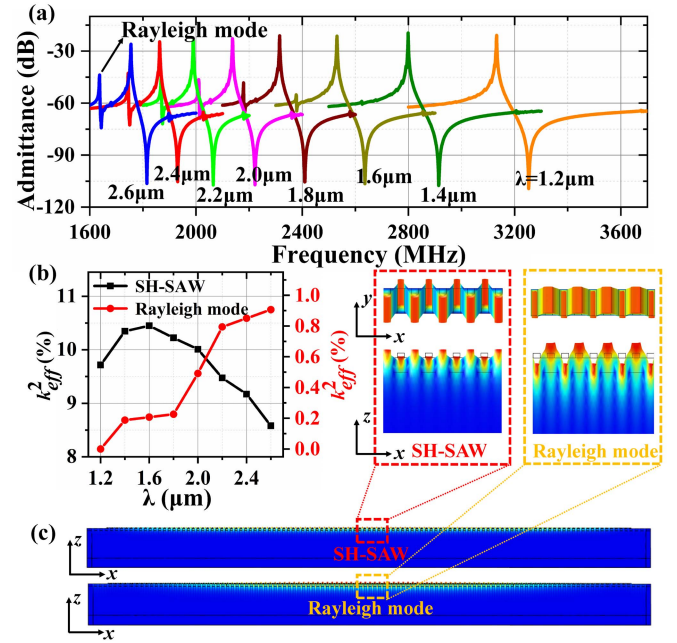


Fig. 5. (a) Simulated admittance curves of SAW resonators on LTOS with different values of λ (~ 1.2 – $2.6 \mu\text{m}$). (b) Extracted k_{eff}^2 of SH-SAW and Rayleigh mode at different values of λ . (c) Cross-sectional view of the displacement mode shapes and zoomed-in images of SH-SAW and Rayleigh mode.

when a proper h_{LT}/λ value (e.g., $h_{\text{LT}}/\lambda = 0.383$) is selected. Note that the Rayleigh spurious response can be weakened but not completely suppressed by optimizing the structural design, such as by reducing the IDT electrode thickness. In addition, replacing the LiTaO₃ in other cuts can effectively suppress the Rayleigh spurious response and may also markedly reduce k_{eff}^2 of the main mode.

IV. EXPERIMENT AND RESULTS

A. Fabrication of the Devices

Based on an LTOS substrate, SAW devices with IDTs and reflectors were fabricated using electron-beam lithography, metal evaporation, and the liftoff process. The thicknesses of the LiTaO₃ layer and the Al/Ti electrode are about 460 and 135 nm, respectively. Fig. 6(a) shows an OM image of a fabricated SH-SAW resonator with $\lambda = 2.6 \mu\text{m}$, while Fig. 6(b) and (c) shows the corresponding top and cross-sectional scanning electron microscope (SEM) images, respectively.

B. Low-Loss SH0 Mode Resonator

The frequency responses of the fabricated acoustic devices were characterized using a vector network analyzer (Keysight E5071C) with a terminal impedance of 50 Ω at room temperature in air. The measured and fitted admittance and Bode- Q curves of the resonator with $\lambda = 2.6 \mu\text{m}$ are shown in Fig. 7(a) and (b), respectively, exhibiting a large admittance ratio of 72 dB, an excellent Q_{max} -value of 3019, a k_{eff}^2 of 5.14, and a figure of merit ($\text{FoM} = k_{\text{eff}}^2 \times Q_{\text{max}}$) of 155 at 1.76 GHz. The excellent Q value indicates low material loss and efficient

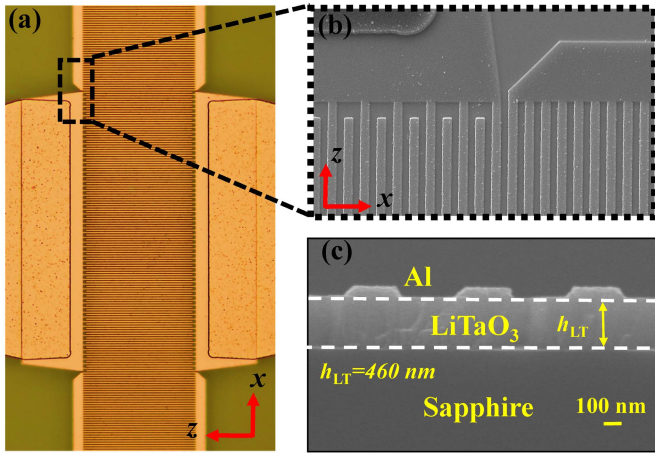


Fig. 6. (a) OM image and (b) top and (c) cross-sectional SEM images of a fabricated resonator.

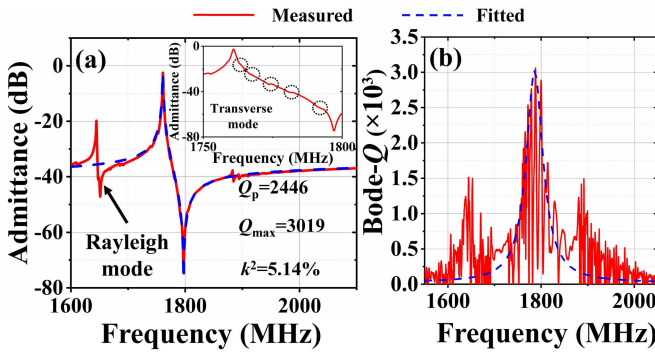


Fig. 7. Measured and fitted (a) admittance curves and (b) Bode- Q curves of a resonator with $\lambda = 2.6 \mu\text{m}$.

TABLE I
COMPARISON OF SH-SAW RESONATORS

Ref.	substrate	f_s (GHz)	Q_p	Q_{\max}	k_{eff}^2 (%)	ML*
[11]	LiTaO ₃ /SiO ₂ /Si	1.9	~2,800	4,000	9.8	Y
[4]	LiNbO ₃ /SiO ₂ /Si	0.83	~250	251	36.5	Y
[5]	LiNbO ₃ /SiO ₂ /SiC	1.32	260	330	28.4	Y
[3]	LiTaO ₃ /SiO ₂ / Poly-Si/Si	1.53	~2,400	6,000	~11.9	Y
This work	LiTaO₃/Sapphire	1.76	2,446	3,019	5.14	N

*ML: Multi-Layer

acoustic energy confinement. Several transverse modes are identified between the resonant and antiresonant frequencies, resulting in a loss of acoustic energy and ripples within the filter passband. Finer device designs, such as flattening the slowness curves [35] or tilting the electrodes [11], could be used to mitigate these modes and a flatter passband and higher Q could be expected. Notably, the values of the extracted k_{eff}^2 are smaller than the simulated ones; this may be attributable to inaccurate material parameters used in the simulation, deviations of electrode thickness, ion implantation-induced damages in the LiTaO₃ thin film, and so on.

A comparison between this work and some other SH-SAW resonators with different substrates [3]–[5], [11] is shown in Table I. The resonator in this work shows quite a high value of Q_{\max} and moderate k_{eff}^2 . In particular, the resonator in this work achieved a very high Q_p , which is the Q value at

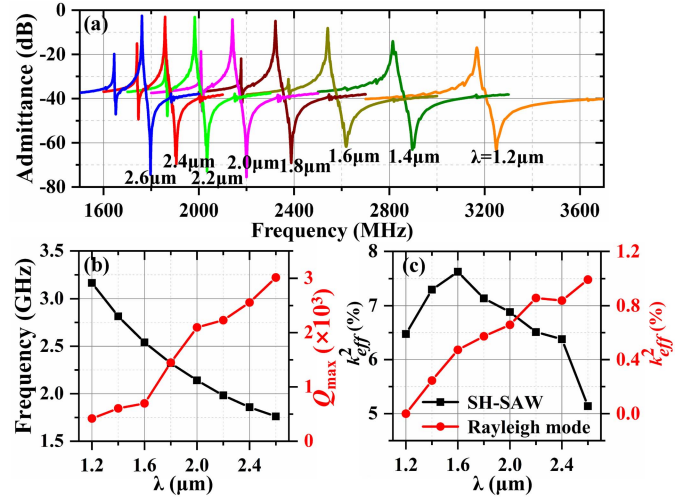


Fig. 8. (a) Measured admittance curves, (b) extracted f_s and Q_{\max} values, and (c) extracted k_{eff}^2 values of resonators with different λ values ranging from 1.2 to 2.6 μm .

the antiresonance frequency. Q_p is calculated by the ratio of the antiresonance frequency to its 3 dB bandwidth ($Q_p = f_p/\Delta f_{3\text{dB}}$) in this case, indicating that both structural loss (acoustic energy leakage) and material loss (e.g., RF loss) of the LTOS-based devices are weak. This result is close to that of I.H.P-SAW [13] and Ultra-SAW [3], and however, an even simpler structure is used in this work. If the design and fabricated process of the LTOS-SAW are optimized, a higher value of Q_{\max} can be expected.

C. High-Order Ladder-Type Filters

Fig. 8(a)–(c) shows the measured admittance curves and the extracted f_s , Q_{\max} , and k_{eff}^2 values of the fabricated resonators with λ ranging from 1.2 to 2.6 μm . Similar to the simulations, a Rayleigh mode with lower f_s appears whose intensity decreases as λ decreases to zero (i.e., $\lambda = 1.2 \mu\text{m}$ and $h/\lambda = 0.383$). k_{eff}^2 of the SH-SAW reaches its maximum value of 7.62% when $\lambda = 1.6 \mu\text{m}$, with the observed variation in k_{eff}^2 mainly caused by the dispersion of SH-SAW in a thin LiTaO₃ plate. Furthermore, as λ decreases, f_s increases and Q_{\max} decreases, with smaller Q_{\max} potentially related to electrical loss.

Based on the measured results of the LTOS-SAW resonators, filters were designed and fabricated. The topology and an OM image of a high-order ladder-type filter are shown in Fig. 9(a) and (b), respectively. A filter with a center frequency (f_c) of 2.2 GHz, an FBW of 2.55%, and a minimum IL (IL_{\min}) of 1.38 dB is shown in Fig. 9(c); this filter also exhibits a Rayleigh mode-induced spurious passband (marked by the orange box). The λ -value of the shunt resonators (λ_{st}) is 2 μm , while that of the series resonators (λ_{ss}) is 1.928 μm . The out-band Rayleigh mode spurious response was mitigated by adjusting the h_{LT}/λ values of the shunt and the series resonators. When λ_{st} and λ_{ss} were set to 1.2 and 1.158 μm , respectively (h_{LT}/λ of 0.383 and 0.397), the filter with an f_c of 3.26 GHz shows a spurious passband-free response, a 3-dB fractional bandwidth (FBW) of 3%, and an IL_{\min} of 2.39 dB,

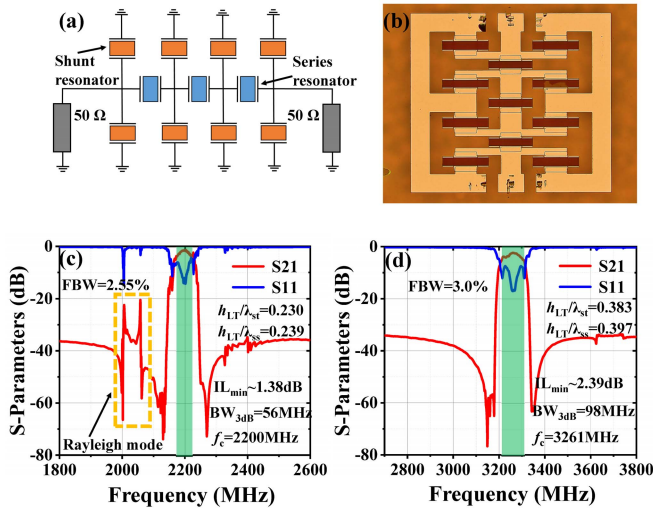


Fig. 9. (a) Topology and (b) OM image of a ladder-type filter. (c) Measured S-parameters of a filter with f_c of 2200 MHz. (d) Measured S-parameters of a filter with f_c of 3261 MHz.

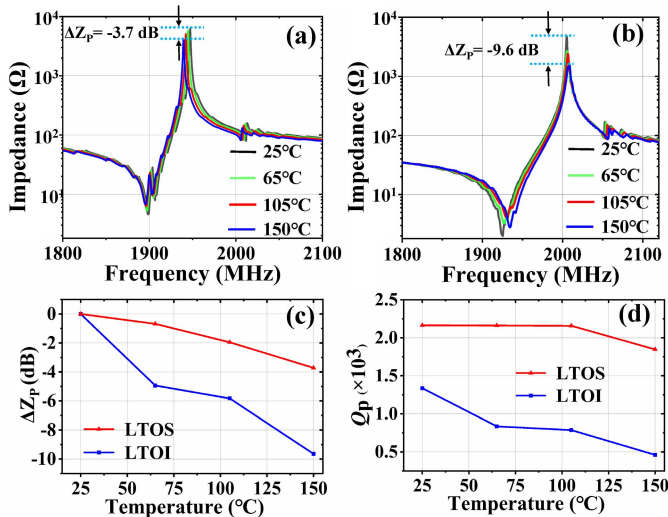


Fig. 10. Temperature characteristics of (a) LTOS-SAW resonator and (b) LTOI-SAW resonator. (c) Impedance variation (ΔZ_p) and (d) Q_p in the temperature range from ~ 25 to 150 °C.

as shown in Fig. 9(d). The performance of the filters can be further improved by optimizing the topology and the fabricated process.

D. Temperature Characteristics of RF Performance

To investigate the temperature characteristics of the LTOS substrate's RF performance, resonators based on LTOS and LTOI_I substrates were tested at temperatures ranging from 25 °C to 150 °C. To achieve similar frequencies, the λ -values of LTOS-SAW and LTOI-SAW were set to 2.4 and 2.0 μm , respectively, and the electrode thickness was set to 120 nm. The temperature characteristics of LTOS-SAW and LTOI-SAW are shown in Fig. 10(a) and (b), respectively. The impedance at the antiresonant frequency (Z_p) of both resonators decreases as the test temperature increases. Fig. 10(c) shows the impedance variation at antiresonance frequencies (ΔZ_p) for the two resonators in the temperature range of ~ 25 °C– 150 °C (a reference temperature of 25 °C).

The impedance attenuation of LTOS is markedly smaller than that of LTOI with increasing test temperature, reaching 3.7 and 9.6 dB for LTOS-SAW and LTOI-SAW at 150 °C, respectively. Fig. 10(d) shows Q_p of the two resonators at different temperatures. Similar to the tested CPW results, both resonators exhibited decreased Q_p with increasing temperature. When the test temperature rose to 150 °C, Q_p of LTOS-SAW decreased from 2164 to 1847 , whereas Q_p of the LTOI-SAW decreased from 1337 to 462 . This result demonstrates that LTOS-SAW still exhibits excellent RF performance at 150 °C, whereas the performance of LTOI-SAW is degraded with increasing temperature.

V. CONCLUSION

In this work, a heterogeneous LTOS substrate with low RF loss was successfully fabricated using an ion-cutting process. Based on the LTOS substrate, the fabricated resonators show scalable resonances from 1.76 to 3.17 GHz, a maximum Q_{max} of 3019 , and an admittance ratio of 72 dB at 1.76 GHz. A filter with f_c of 3.26 GHz and a 3 -dB FBW of 3% shows a spurious passband-free response. With further optimization of the ion-cutting process and device design, a recovered k_{eff}^2 and a higher Q value can be expected. Compared to LTOI, the CPW built on LTOS exhibits much smaller IL values, while the SH-SAW resonator presents lower impedance attenuation with increasing test temperature. The low RF loss and stable temperature characteristics of the LTOS substrate are attributed to the sapphire's extremely high resistivity, in addition to the excellent thermal stability of the LiTaO₃/sapphire interface. Thus, the findings of this study indicate that LTOS-SAW devices show excellent potential for applications in RF wireless communication devices.

ACKNOWLEDGMENT

The authors would like to thank the Fudan Nano-fabrication Laboratory and ShanghaiTech Quantum Device Laboratory (SQDL) for device fabrication support.

REFERENCES

- [1] K.-Y. Hashimoto *et al.*, "Recent development of temperature compensated SAW devices," in *Proc. IEEE Int. Ultrason. Symp.*, Oct. 2011, pp. 79–86, doi: [10.1109/ULTSYM.2011.0021](https://doi.org/10.1109/ULTSYM.2011.0021).
- [2] T. Takai, H. Iwamoto, Y. Takamine, H. Yamazaki, and N. Nakajima, "High-performance SAW resonator on new multilayered substrate using LiTaO₃ crystal," *IEEE Trans. Ultrason., Ferroelectr., Freq. Control*, vol. 64, no. 9, pp. 1382–1389, Sep. 2017, doi: [10.1109/TUFFC.2017.2738119](https://doi.org/10.1109/TUFFC.2017.2738119).
- [3] E. Butaud, S. Ballandras, M. Bousquet, A. Drouin, and A. Reinhardt, "Innovative smart cut piezo on insulator (POI) substrates for 5G acoustic filters," in *IEDM Tech. Dig.*, Dec. 2020, p. 34, doi: [10.1109/IEDM13553.2020.9372020](https://doi.org/10.1109/IEDM13553.2020.9372020).
- [4] T.-H. Hsu, K.-J. Tseng, and M.-H. Li, "Large coupling acoustic wave resonators based on LiNbO₃/SiO₂/Si functional substrate," *IEEE Electron Device Lett.*, vol. 41, no. 12, pp. 1825–1828, Dec. 2020, doi: [10.1109/LED.2020.3030797](https://doi.org/10.1109/LED.2020.3030797).
- [5] J. Shen *et al.*, "High-performance surface acoustic wave devices using LiNbO₃/SiO₂/SiC multilayered substrates," *IEEE Trans. Microw. Theory Techn.*, vol. 69, no. 8, pp. 3693–3705, Aug. 2021, doi: [10.1109/TMTT.2021.3077261](https://doi.org/10.1109/TMTT.2021.3077261).
- [6] S. Zhang *et al.*, "Surface acoustic wave devices using lithium niobate on silicon carbide," *IEEE Trans. Microw. Theory Techn.*, vol. 68, no. 9, pp. 3653–3666, Sep. 2020, doi: [10.1109/TMTT.2020.3006294](https://doi.org/10.1109/TMTT.2020.3006294).
- [7] H. Zhou *et al.*, "Surface wave and Lamb wave acoustic devices on heterogeneous substrate for 5G front-ends," in *IEDM Tech. Dig.*, Dec. 2020, p. 17, doi: [10.1109/IEDM13553.2020.9372128](https://doi.org/10.1109/IEDM13553.2020.9372128).

- [8] S. Gong, "Lithium niobate for M/NEMS resonators," in *Piezoelectric MEMS Resonators*, H. Bhugra and G. Piazza, Eds. Cham, Switzerland: Springer, 2017, pp. 99–129.
- [9] A. Hagelauer, G. Fattinger, C. C. W. Ruppel, M. Ueda, K. Hashimoto, and A. Tag, "Microwave acoustic wave devices: Recent advances on architectures, modeling, materials, and packaging," *IEEE Trans. Microw. Theory Techn.*, vol. 66, no. 10, pp. 4548–4562, Oct. 2018, doi: [10.1109/TMTT.2018.2854160](https://doi.org/10.1109/TMTT.2018.2854160).
- [10] S. Inoue and M. Solal, "Layered SAW resonators with near-zero TCF at both resonance and anti-resonance," in *Proc. IEEE Int. Ultrason. Symp. (IUS)*, Oct. 2019, pp. 2079–2082, doi: [10.1109/ULTSYM.2019.8925592](https://doi.org/10.1109/ULTSYM.2019.8925592).
- [11] H. Iwamoto, T. Takai, Y. Takamine, T. Nakao, T. Fuyutsume, and M. Koshino, "Transverse modes in I.H.P. SAW resonator and their suppression method," in *Proc. IEEE Int. Ultrason. Symp. (IUS)*, Oct. 2018, pp. 1–4, doi: [10.1109/ULTSYM.2018.8580175](https://doi.org/10.1109/ULTSYM.2018.8580175).
- [12] T. Takai, H. Iwamoto, Y. Takamine, H. Yamazaki, and N. Nakajima, "Incredible high performance SAW resonator on novel multi-layered substrate," in *Proc. IEEE Int. Ultrason. Symp. (IUS)*, Tours, France, Sep. 2016, pp. 1–4, doi: [10.1109/ULTSYM.2016.7728455](https://doi.org/10.1109/ULTSYM.2016.7728455).
- [13] T. Kimura, M. Omura, Y. Kishimoto, and K. Hashimoto, "Comparative study of acoustic wave devices using thin piezoelectric plates in the 3–5-GHz range," *IEEE Trans. Microw. Theory Techn.*, vol. 67, no. 3, pp. 915–921, Mar. 2019, doi: [10.1109/TMTT.2018.2890661](https://doi.org/10.1109/TMTT.2018.2890661).
- [14] D. Lederer and J.-P. Raskin, "Effective resistivity of fully-processed SOI substrates," *Solid-State Electron.*, vol. 49, no. 3, pp. 491–496, 2005, doi: [10.1016/j.sse.2004.12.003](https://doi.org/10.1016/j.sse.2004.12.003).
- [15] H. S. Gamble, B. M. Armstrong, S. J. N. Mitchell, Y. Wu, V. F. Fusco, and J. A. C. Stewart, "Low-loss CPW lines on surface stabilized high-resistivity silicon," *IEEE Microw. Guided Wave Lett.*, vol. 9, no. 10, pp. 395–397, Oct. 1999, doi: [10.1109/75.798027](https://doi.org/10.1109/75.798027).
- [16] D. Lederer and J.-P. Raskin, "New substrate passivation method dedicated to HR SOI wafer fabrication with increased substrate resistivity," *IEEE Electron Device Lett.*, vol. 26, no. 11, pp. 805–807, Nov. 2005, doi: [10.1109/LED.2005.857730](https://doi.org/10.1109/LED.2005.857730).
- [17] W. Heinrich, "Quasi-TEM description of MMIC coplanar lines including conductor-loss effects," *IEEE Trans. Microw. Theory Techn.*, vol. 41, no. 1, pp. 45–52, Jan. 1993, doi: [10.1109/22.210228](https://doi.org/10.1109/22.210228).
- [18] C. R. Neve and J.-P. Raskin, "RF harmonic distortion of CPW lines on HR-Si and trap-rich HR-Si substrates," *IEEE Trans. Electron Devices*, vol. 59, no. 4, pp. 924–932, Apr. 2012, doi: [10.1109/TED.2012.2183598](https://doi.org/10.1109/TED.2012.2183598).
- [19] Y. Wu, H. S. Gamble, B. M. Armstrong, V. F. Fusco, and J. A. C. Stewart, "SiO₂ interface layer effects on microwave loss of high-resistivity CPW line," *IEEE Microw. Guided Wave Lett.*, vol. 9, no. 1, pp. 10–12, Jan. 1999, doi: [10.1109/75.752108](https://doi.org/10.1109/75.752108).
- [20] D. A. Feld, R. Parker, R. Ruby, P. Bradley, and S. Dong, "After 60 years: A new formula for computing quality factor is warranted," in *Proc. IEEE Ultrason. Symp.*, Nov. 2008, pp. 431–436, doi: [10.1109/ULTSYM.2008.0105](https://doi.org/10.1109/ULTSYM.2008.0105).
- [21] E. Butaud, B. Ta Vel, S. Ballandras, M. Bousquet, and I. Bertrand, "Smart cut piezo on insulator (POI) substrates for high performances SAW components," in *Proc. IEEE Int. Ultrason. Symp. (IUS)*, Sep. 2020, pp. 1–4, doi: [10.1109/IUS46767.2020.9251517](https://doi.org/10.1109/IUS46767.2020.9251517).
- [22] Y.-H. Song and S. Gong, "Spurious mode suppression in SH₀ lithium niobate laterally vibrating MEMS resonators," in *IEDM Tech. Dig.*, Dec. 2015, p. 18, doi: [10.1109/IEDM.2015.7409728](https://doi.org/10.1109/IEDM.2015.7409728).
- [23] M. Kadota and S. Tanaka, "Ultra-wideband ladder filter using SH₀ plate wave in thin LiNbO₃ plate and its application to tunable filter," *IEEE Trans. Ultrason., Ferroelectr., Freq. Control*, vol. 62, no. 5, pp. 939–946, May 2015, doi: [10.1109/TUFFC.2014.006845](https://doi.org/10.1109/TUFFC.2014.006845).
- [24] R. Lu, Y. Yang, S. Link, and S. Gong, "Enabling higher order Lamb wave acoustic devices with complementarily oriented piezoelectric thin films," *J. Microelectromech. Syst.*, vol. 29, no. 5, pp. 1332–1346, Oct. 2020, doi: [10.1109/JMEMS.2020.3007590](https://doi.org/10.1109/JMEMS.2020.3007590).
- [25] V. Plessky *et al.*, "Laterally excited bulk wave resonators (XBARs) based on thin lithium niobate platelet for 5 GHz and 13 GHz filters," in *IEEE MTT-S Int. Microw. Symp. Dig.*, Jun. 2019, pp. 512–515, doi: [10.1109/MWSYM.2019.8700876](https://doi.org/10.1109/MWSYM.2019.8700876).
- [26] T. D. Ha and J. Bao, "Reducing anchor loss in thin-film aluminum nitride-on-diamond contour mode MEMS resonators with support tethers based on phononic crystal strip and reflector," *Microsyst. Technol.*, vol. 22, no. 4, pp. 791–800, Apr. 2016, doi: [10.1007/s00542-015-2678-1](https://doi.org/10.1007/s00542-015-2678-1).
- [27] A. Gao, K. Liu, J. Liang, and T. Wu, "AlN MEMS filters with extremely high bandwidth widening capability," *Microsyst. Nanoeng.*, vol. 6, no. 1, p. 74, Dec. 2020, doi: [10.1038/s41378-020-00183-5](https://doi.org/10.1038/s41378-020-00183-5).
- [28] M. Gorisse *et al.*, "High frequency LiNbO₃ bulk wave resonator," in *Proc. Joint Conf. IEEE Int. Freq. Control Symp. Eur. Freq. Time Forum (EFTF/IFC)*, Apr. 2019, pp. 1–2, doi: [10.1109/FCS.2019.8856017](https://doi.org/10.1109/FCS.2019.8856017).
- [29] M. Bousquet *et al.*, "Single-mode high frequency LiNbO₃ film bulk acoustic resonator," in *Proc. IEEE Int. Ultrason. Symp. (IUS)*, Oct. 2019, pp. 84–87, doi: [10.1109/ULTSYM.2019.8925617](https://doi.org/10.1109/ULTSYM.2019.8925617).
- [30] Y. Yan, K. Huang, H. Zhou, X. Zhao, and X. Ou, "Wafer-scale fabrication of 42° rotated Y-cut LiTaO₃-on-insulator (LTOI) substrate for a SAW resonator," *ACS Appl. Electron. Mater.*, vol. 1, no. 8, pp. 1660–1666, Aug. 2019, doi: [10.1021/acsaelm.9b00351](https://doi.org/10.1021/acsaelm.9b00351).
- [31] T. L. Chua, M. Kadota, and S. Tanaka, "Low velocity HAL SAW resonator using LiNbO₃ thin plate on quartz substrate," in *Proc. Joint Conf. Eur. Freq. Time Forum IEEE Int. Freq. Control Symp. (EFTF/IFCS)*, Jul. 2021, pp. 1–3, doi: [10.1109/EFTF/IFCS52194.2021.9604287](https://doi.org/10.1109/EFTF/IFCS52194.2021.9604287).
- [32] J. Wu *et al.*, "Low-loss SAW devices with LiTaO₃ on extremely high resistance substrate," in *Proc. IEEE Int. Ultrason. Symp. (IUS)*, Sep. 2021, pp. 1–4, doi: [10.1109/IUS52206.2021.9593793](https://doi.org/10.1109/IUS52206.2021.9593793).
- [33] M. Miura *et al.*, "Temperature compensated LiTaO₃/sapphire bonded SAW substrate with low loss and high coupling factor suitable for U.S.-PCS application," in *Proc. IEEE Ultrason. Symp. (IUS)*, vol. 2, Aug. 2004, pp. 1322–1325, doi: [10.1109/ULTSYM.2004.1418036](https://doi.org/10.1109/ULTSYM.2004.1418036).
- [34] S. Gong and G. Piazza, "Design and analysis of lithium–niobate-based high electromechanical coupling RF-MEMS resonators for wideband filtering," *IEEE Trans. Microw. Theory Techn.*, vol. 61, no. 1, pp. 403–414, Jan. 2013, doi: [10.1109/TMTT.2012.2228671](https://doi.org/10.1109/TMTT.2012.2228671).
- [35] S. Inoue and M. Solal, "LT/quartz layered SAW substrate with suppressed transverse mode generation," in *Proc. IEEE Int. Ultrason. Symp. (IUS)*, Sep. 2020, pp. 1–4, doi: [10.1109/IUS46767.2020.9251459](https://doi.org/10.1109/IUS46767.2020.9251459).